Available online at www.sciencedirect.com

ScienceDirect

Ceramics International 40 (2014) 357–366

CERAMICS INTERNATIONAL

www.elsevier.com/locate/ceramint

Analysis of the complex permeability of NiCuZn ferrites up to 1 GHz with regard to Cu content and sintering temperature

C.A. Stergiou*, V. Zaspalis

Laboratory of Inorganic Materials, Centre for Research and Technology Hellas, Thessaloniki 57001, Greece

Received 30 April 2013; received in revised form 3 June 2013; accepted 4 June 2013
Available online 18 June 2013

Abstract

We have studied the frequency dependent permeability of $Ni_{0.60-x}Cu_xZn_{0.40}Fe_{1.98}O_4$ ferrites ($x=0$, 0.10, 0.20, 0.30) with regard to the Cu concentration and the undergone heat treatment. To this end, single-phase magnetic ceramics were prepared and characterized in terms of the reversible complex permeability $\mu^*(f)$ in the 100 kHz to 1 GHz frequency range. The $\mu^*(f)$ spectra are analyzed into three elementary magnetization processes with changing weight factors as Cu content or sintering temperature T_{SINT} increase. In fact, in addition to the spin rotation relaxation at 150–400 MHz we initially identify the contribution from reversible domain wall bowing rising at 20–80 MHz. For higher Cu content or T_{SINT}, the latter mechanism is suppressed to the benefit of reversible wall displacement in the range below 1 MHz. Concerning particularly the domain wall motion, system dynamics theory and least-squares curve fitting of $\mu^*(f)$ spectra were employed to distinguish between the high-frequency underdamped resonance (d. wall bowing) and the lower frequency overdamped relaxation dispersions (d. wall displacement). This distinction originates in the microstructural variance between the pinned low-energy domain walls in individual small grains and the cooperative rigid high-energy walls in large grains, respectively. The relevant transition of morphology in NiCuZn ferrites, induced by Cu substitution or by high T_{SINT}, is identified through SEM observation and accords with the experimental results of dilatometry and density measurements. The remarked densification process is reflected on the increase of initial permeability as well. Moreover, on the basis of the recorded B–H loops we derive that the maximum induction B_{MAX} follows the density variation of sintered specimens, contrarily to the coercive field H_C which is significantly decreased when magnetic domain walls appear.
© 2013 Elsevier Ltd and Techna Group S.r.l. All rights reserved.

Keywords: D. Ferrites; Cu substitution; Complex permeability; Domain wall relaxation and resonance

1. Introduction

The introduction of Cu in the composition of cubic ferrites is a typical materials design technique in pursue of low-temperature densification [1,2]. This effect commences most probably due to the lattice diffusion of Cu ions [3,4] and is reinforced by the formation of a CuO phase at grain boundaries [5]. As a result, NiCuZn ferrites may be produced by low-temperature firing, whereas they additionally exhibit good electromagnetic properties in relatively high frequencies [6]. Furthermore, taking into account the economic aspect of ferrites manufacturing, we recognize the benefits gained by substituting Ni with Cu in the already massively produced NiZn ferrites. These special characteristics of NiCuZn spinels render them suitable for the fabrication of integrated planar electronic components (inductors, LC filters and transformers) compatible with microelectronics and surface mount technology (SMT) [7,8] and of EMI suppressing films operating in the 100 MHz to 1 GHz region [9,10].

With regard to the dynamic magnetic properties of ferrites, three basic reversible magnetization processes are discerned. Specifically, according to magnetic materials theory the magnetization under a low ac field is achieved through the rotation of magnetic moments within a domain along with the vibration and displacement of formed domain walls [11,12]. However, ambiguity rises about the origin and the type of domain wall motion as the latter mechanism is either not employed in the research of spinel ferrites or not further

*Corresponding author. Tel.: +30 2310 498244; fax: +30 2310 498131.
E-mail addresses: stergiou@cperi.certh.gr, stergiou.babis@gmail.com (C.A. Stergiou).

0272-8842/$ - see front matter © 2013 Elsevier Ltd and Techna Group S.r.l. All rights reserved.
http://dx.doi.org/10.1016/j.ceramint.2013.06.010

analyzed [13–15]. As the comprehension of frequency dependent magnetization processes in such magnetic ceramics is essential to design low-loss end products with tailored magnetic response, we have prepared and analyzed a set of NiCuZn ferrites in terms of their complex permeability in the 100 kHz to 1 GHz frequency range.

2. Materials and methods

The set of polycrystalline cubic ferrites that was selected for the present study is described by the nominal composition $Ni_{0.60-x}Cu_xZn_{0.40}Fe_{1.98}O_4$ with x=0, 0.10, 0.20 and 0.30 (samples N0, N1, N2 and N3 respectively). Since we intend to focus on the effects of Cu substitution for Ni, the Zn content was kept constant and equal to 0.40, which is expected to yield relatively high values of magnetization [11]. Additionally, Fe coefficient was adjusted to 1.98, which is reduced from the stoichiometric coefficient, as that promotes densification [3,5,16]. Despite the extent of the past research on NiCuZn ferrites, no relevant electromagnetic study on these specific compounds has been published.

The samples under test were prepared with the conventional solid-state reaction method starting from the proper oxides (NiO, CuO, ZnO and Fe_2O_3). The needed amounts of the precursors were initially ball mixed for 3 h in deionized water and dried at 100 °C for 24 h, followed by a heat treatment at 750 °C for 2 h with a heating rate of 5 °C/min. The prefired powder mixtures were further ball milled for 3 h and dried at 100 °C for 24 h and subsequently granulated with the addition of a plasticizer and lubricant compound (polyvinyl alcohol and Zn stearate, respectively). The granulated samples were then pressed under axial compaction (1350 psi) to form toroidal samples (outer/inner diameter: 23.5 mm/14.5 mm) with approximately 3 gr/cm^3 green density. Finally, in order to monitor the effect of sintering top temperature on certain properties of the end products, the ring-shaped samples were annealed for 3 h in air at temperatures varying from 1000 °C to 1200 °C.

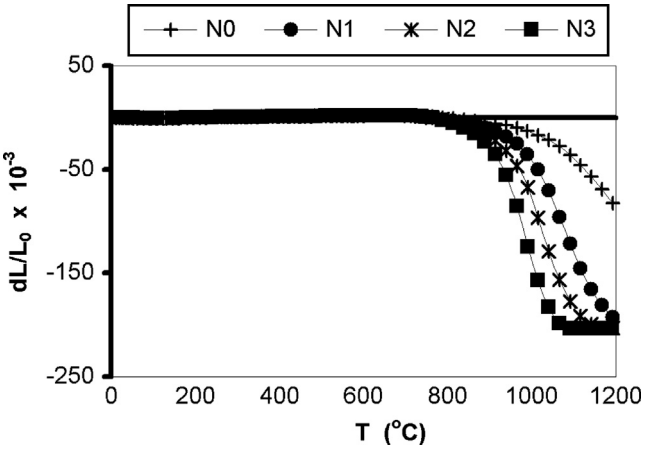

Fig. 1. Relative lengths change of prefired rods N0, N1, N2 and N3 with temperature.

For the phase and crystal structure identification of both prefired and sintered samples, the X-ray diffraction patterns were recorded (powder diffractometer Siemens D-500, CuKa). Moreover, the prefired powders were examined in terms of their particle size distribution (Malvern Mastersizer-S), whereas the shrinkage of pressed cylinders during annealing was measured by dilatometry performed up to 1200 °C (horizontal pushrod dilatometer Netzsch DIL 402PC). The microstructure of the sintered samples was studied by means of JEOL JSM6300 scanning electron microscope. Concerning the magnetic properties of these NiCuZn materials, we measured the B–H loops (10 kHz, maximum magnetic field 1200 A/m), the initial permeability (10 kHz, flux density 0.1 mT) and the complex permeability spectrum in the frequency range 100 kHz–1 GHz. All the magnetic measurements up to 1 MHz were conducted with an automated measurement apparatus which comprises Agilent 4284A Precision LCR meter, Tektronix TDS-714L Oscilloscope, Agilent 33120A frequency generator and the appropriate HF and RF amplifiers. For complex permeability measurements at frequencies from 1 MHz to 1 GHz, the Agilent E4991A RF Impedance Material Analyzer was used.

3. Results

3.1. Dilatometric, structural, and morphological characterization

Dilatometry is used to characterize the rod specimens of compacted prefired ferrite granules. By measuring the relative elongation/shrinkage along the longitudinal axis of rods during heating, useful information can be obtained regarding the densification and sintering process. Specifically, Fig. 1 depicts the measured length variation dL of the cylinders, normalized to their initial length L_0, with temperature up to 1200 °C. As a result, we initially derive that by increasing the Cu content either higher shrinkage is attained at the same heating temperature, or conversely, lower heating temperature is needed for the same shrinkage. In Table 1 we report the temperature where shrinkage first appears T_{INI} and the temperature of maximum shrinkage rate (maximum densification) T_{MAX}, which was extracted from the derivatives of the curves.

Table 1
Shrinkage parameters derived from dilatometry characterization. Here, T_{INI} and T_{MAX} are the temperatures where shrinkage begins and its rate is maximized, respectively.

	N0 (Cu: 0)	N1 (Cu: 0.10)	N2 (Cu: 0.20)	N3 (Cu: 0.30)
T_{INI} (°C)	661.9	661.8	662.0	661.9
T_{MAX} (°C)	1200	1058.8	1017.2	970.5

The tabulated values show that as Cu amount is increased, T_{INI} remains practically constant (662 °C), whereas T_{MAX} is reduced from above 1200 °C for N0 (Cu: 0) down to 970.5 °C for N3 (Cu: 0.30). The latter quantity is very important for ferrite processing as it defines the optimal range of temperatures where a balance of sufficient density and appropriate microstructure is achieved. The sequential changes of microstructure with Cu or annealing temperature will further be discussed in conjunction with the measured density and SEM observation.

The structural investigation of the prefired powders of NiCuZn ferrites was conducted by means of XRD analysis. According to the recorded XRD patterns, all the prefired compounds are of high crystallinity and mainly comprise spinel ferrite as the dominant phase. Actually, the crystal structure was identified as that of $Ni_{0.50}Zn_{0.50}Fe_2O_4$ (JCPDS no. 52-0278), yet in the cases of no or low Cu content (N0 and N1) traces of hematite Fe_2O_3 appeared as well. However, after sintering at high temperatures (1000–1200 °C) the formation of ferrite structure was completed and all the samples appeared to be single phase spinels, as the concentration of any secondary phases is below the XRD detection limit. In Fig. 2 the XRD patterns of ferrites N0–N3 sintered at 1100 °C are displayed. Apart from the monophase nature of the samples, we may additionally notice the shift of the diffraction patterns to lower angles with the raise of Cu. This effect is attributed to the expected growth of unit cell constant a due to the substitution of Ni^{2+} ions by the larger Cu^{2+} ions in the lattice [17].

The density d of soft magnetic ceramics is a critical parameter as, in combination with other microstructural features, it largely determines their electromagnetic properties. The variation of the measured density of toroids with sintering top temperature (T_{SINT}) is demonstrated in Fig. 3 for all four different compounds. Taking into account the common basis of all the prefired powders in terms of press density and particle distribution (average values: $D_{10}=0.28$ μm, $D_{50}=0.87$ μm and $D_{90}=4.94$ μm), we may reasonably attribute the observed d–T_{SINT} variation to chemical composition. Specifically, the substitution of Ni by Cu clearly and expectedly promotes densification as it shifts d–T_{SINT} curves to lower temperatures. In correspondence with the dilatometry results,

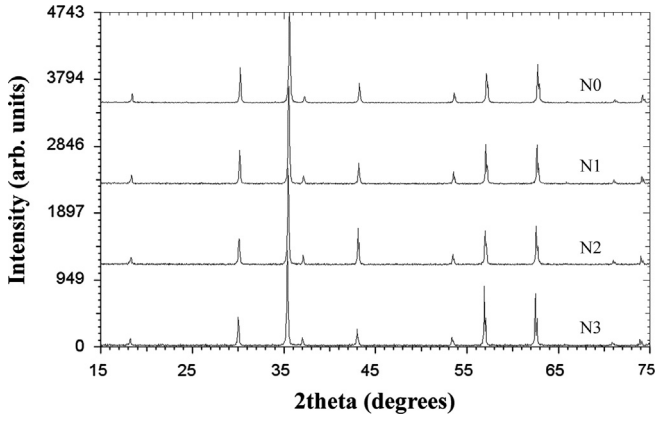

Fig. 2. XRD patterns of samples N0, N1, N2 and N3 (Cu: 0, 0.10, 0.20 and 0.30) sintered at 1100 °C.

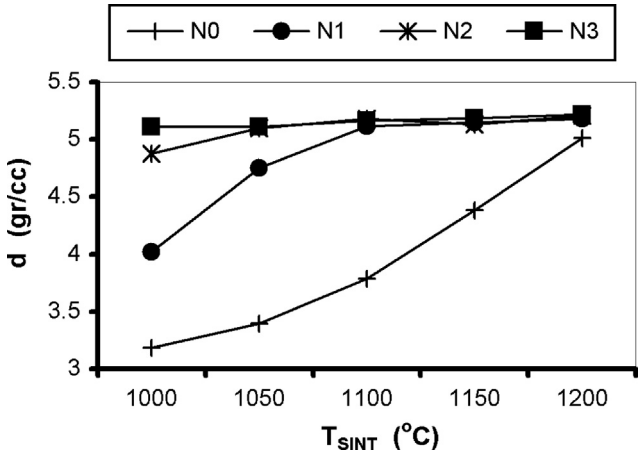

Fig. 3. Densities of sintered toroids N0, N1, N2 and N3 with sintering temperatures.

we conclude that the increase of Cu/Ni ratio in NiZn ferrites finally induces either higher density for the same T_{SINT}, or a lower required T_{SINT} to achieve the same density value.

Concerning the shape of the d–T_{SINT} curves, it appears that they basically constitute sections of sigmoid-like functions. Specifically, for relatively low-temperature sintering we get low-density ceramics due to imperfect microstructure and high intergranular porosity. As T_{SINT} further increases, the intergranular pores are substantially diminished and grains are uniformly developed, maximizing the densification rate (this state is commonly defined as the normal microstructure). Finally, above this temperature range, microstructure with either duplex structure or exaggerated-discontinuous grain growth usually takes place [18]. In both cases, enhanced porosity is created inside the large grains (intragranular pores) and this probably contributes to the observed drop of the densification rate and the fluctuation of the density values above 5 gr/cm^3.

The described connection of density and morphology with the composition and T_{SINT} is illustrated in Fig. 4a–e, taken by SEM observation of the samples N0, N1, N2 and N3 sintered at 1100 °C and the sample N2 sintered at 1000 °C, respectively. Actually, starting from a low-density NiZn ferrite with submicron grains (N0), the addition of Cu initially enhances densification due to grain growth and decrease of intergranular pores (N1), whereas higher Cu content excites duplex microstructure (N2) and exaggerated grains (N3) in combination with extensive intragranular porosity. Furthermore, by comparing the two N2 samples sintered at 1000 °C and 1100 °C (Fig. 4e and c, respectively), we confirm the existence of optimal heating conditions provoking the development of normal microstructure as well as the deleterious effect of high T_{SINT} on that.

3.2. Magnetic characterization

The ac hysteresis loops of the fabricated toroids were recorded up to the maximum magnetic field intensity of 1200 A/m and narrow loops, typical of soft ferrimagnetic

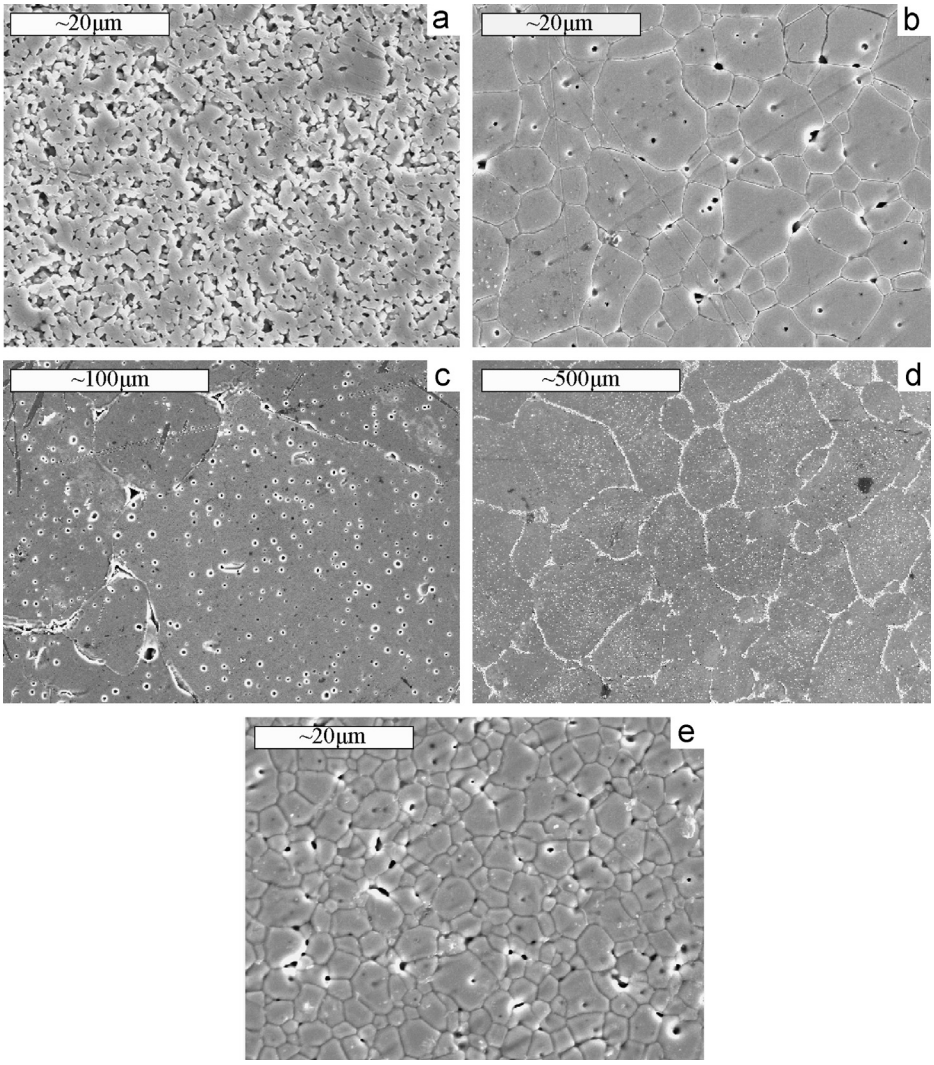

Fig. 4. SEM images of sintered (a) N0, (b) N1, (c) N2, (d) N3 at 1100 °C and (e) N2 at 1000 °C.

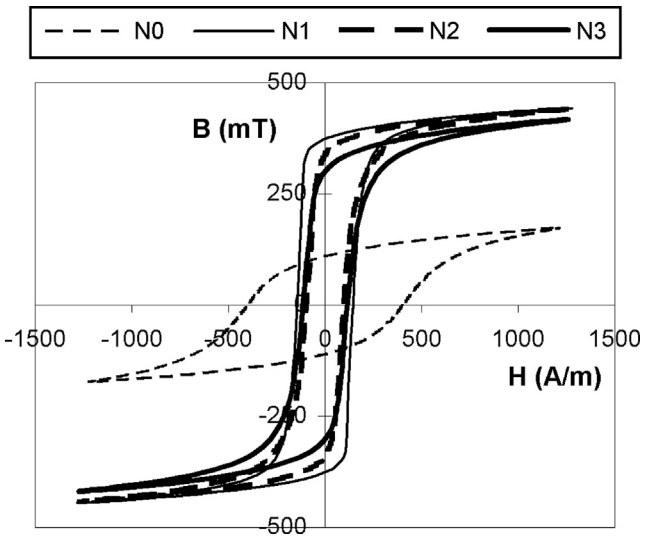

Fig. 5. Hysteresis loops of samples N0, N1, N2 and N3 sintered at 1100 °C.

materials, are obtained for the substituted compounds N1, N2 and N3. On the contrary, the unsubstituted ferrite N0 displays different hysteresis characteristics with lower maximum flux density (B_{MAX}) and generally stronger coercivity (H_C), especially when sintered up to 1150 °C. We indicatively present the *B–H* loops of all samples sintered at 1100 °C in Fig. 5. The remarked magnetic features of ferrite N0 are attributed to the lower density and the incomplete microstructure, which give rise to high demagnetizing fields and low induction.

Concerning the variation of B_{MAX} with T_{SINT}, we would expect that it follows the variation of density, as it is strongly affected by the extent of the magnetic material packing in a specified volume. In fact, this relation is verified by the experimental values demonstrated in Fig. 6a. Additionally, for N1 and N2, whose curve maxima appear in the tested range of T_{SINT}, it is noted that the maximum value of B_{MAX} is diminishing for higher Cu amount. This probably corresponds with the decrease of spontaneous magnetization per formula

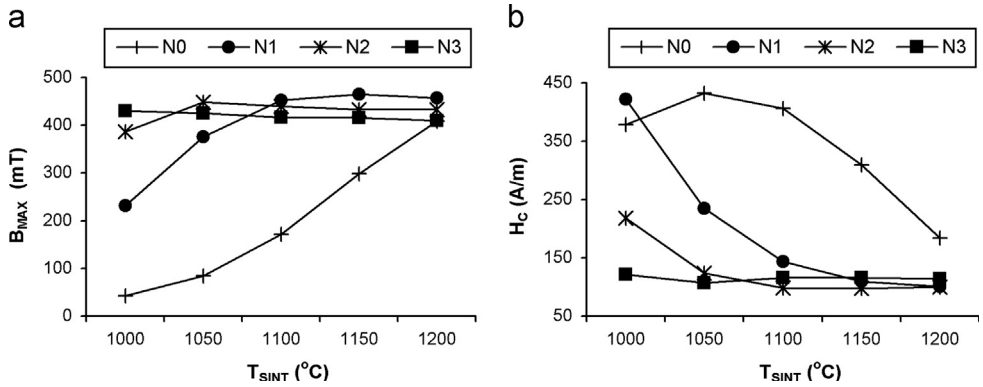

Fig. 6. Variation of (a) maximum flux density B_{MAX} and (b) coercive field H_C of samples N0, N1, N2 and N3 with sintering temperature.

unit, which stems from the lower magnetic moment of Cu^{2+} (1 μ_B) ions compared to that of Ni^{2+} (2 μ_B), considering that both ions occupy octahedral B-sites [11].

In order to understand the variation of coercive field H_C with T_{SINT}, we shall focus on the unsubstituted ferrite N0 (Fig. 6b). As the chemical composition remains unchanged, coercivity shows a striking dependence on morphology and especially on the increasing grain size with T_{SINT}. For N0 material annealed at 1000 °C the grains are assumed to be in single domain state, yet above superparamagnetic range, therefore coercive field, H_C, grows with the occupied volume and grain size [19]. This occurs up to 1050 °C, where coercivity goes through a maximum of 435 A/m followed by a gradual decrement to 183 A/m for T_{SINT}=1200 °C. The observed peak is ascribed to the transition from single-domain to larger multiple-domain particles, which facilitate the magnetization reversal and consequently reduce H_C. On the basis of this analysis, we may notice that all Cu-substituted compositions (N1, N2 and N3) comprise grains large enough to foster the formation of multiple domains in the whole range of T_{SINT} from 1000 °C to 1200 °C.

Fig. 7 demonstrates the generally increasing trend of initial permeability (μ_i) of the fabricated ferrites with T_{SINT}. It also shows that, the addition of Cu in our compounds results in higher permeability for the same T_{SINT} values, whereas it diminishes the required temperature to attain high μ_i. Regarding the origin of initial permeability, it is suggested that it mainly stems from the reversible bulging of domain walls, rather than the domain wall displacement or spin rotation processes [20]. However, as it will be discussed later, in the materials under study the contribution of reversible wall vibration is interestingly suppressed to the benefit of reversible wall displacement mechanism, as the Cu content and T_{SINT} are raised. Independently of the precise predominant domain wall process, the multi-domain grain growth, promoted by higher Cu substitution or T_{SINT}, leads to the cumulative increase in μ_i. Still, the gradient of μ_i variation is restrained in case of sintering N1, N2 and N3 at higher temperature. This decline in the slope of μ_i is most probably induced by the embedded intragranular porosity along with the chemical and morphological imperfections, which have been identified in some similar NiCuZn ferrites [4]. Thus, both magnetization processes of the domain wall bulging and displacement are partially hindered.

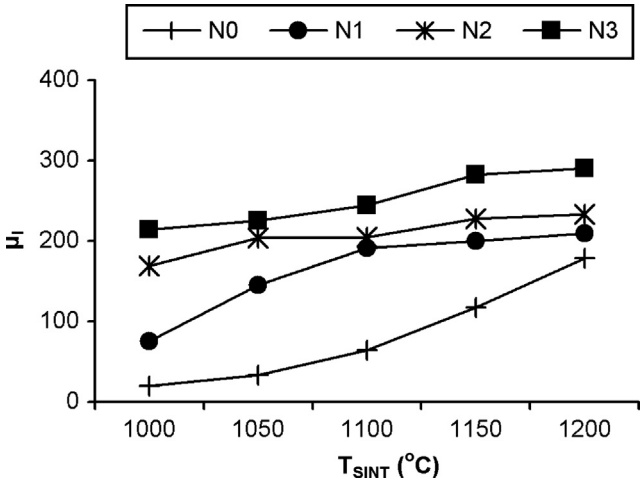

Fig. 7. Variation of initial permeability of samples N0, N1, N2 and N3 with sintering temperature.

3.3. Frequency dependent permeability

As it is already mentioned, the frequency dispersion of permeability in ferrites is determined by three basic reversible magnetization processes, namely the spin magnetization rotation, the domain wall bulging and the domain wall movement [12]. These mechanisms are characterized by different time constants; hence they influence different areas of the frequency spectrum. As the main objective of the present study is to probe into the permeability dispersion of materials, we deem it appropriate to concisely set the theoretical principles of our analysis.

To describe the precession of magnetization vector ($\vec{M}$), for the case of an individual magnetic dipole subjected to an ac magnetic field (H), the Landau–Lifshitz equation modified by Gilbert is the most widely used dynamic approach and is written as [21]

$$\frac{d\vec{M}}{dt} = -\gamma(\vec{M}\vec{H}) + \frac{\lambda}{M}\left(\vec{M}\frac{d\vec{M}}{dt}\right) \quad (1)$$

where γ is the gyromagnetic ratio and λ a dimensionless phenomenological damping coefficient, whose increase signifies higher energy dissipation and results in the reduction of the precession angle. The respective complex reversible

permeability $\mu^*_{sp}(f)$ is calculated as [22]

$$\mu^*_{sp}(f) = \frac{\chi_{0sp}(1 + j\lambda f/f_R)}{(1 + jf/f_R)^2 - (f/f_R)^2} \quad (2)$$

This equation represents a resonance-type dispersion (Lorentzian-type), where χ_{sp0} is the static susceptibility and f_R the ferromagnetic resonance frequency. Here, f_R is determined by the elementary formula of ferromagnetism $2\pi f_R = \gamma H_{eff}$ as proportional to the static effective anisotropy field H_{eff} originating either in structure (magnetocrystalline anisotropy) or morphology (shape anisotropy). Regarding the initial susceptibility generated by the discussed magnetization process, it is proportional to saturation magnetization squared (M_S^2) and to the reciprocal of effective anisotropy [21]. Taking into account the enhanced spin motion damping in actual polycrystalline magnetic ceramics, the parameter λ could be larger than unity [23]. In this case, Eq. (2) for permeability constitutes a relaxation-type frequency dependent variation (Debye-type) with characteristic frequency $f_{sp} = f_R/(2\lambda)$.

Additionally, when the magnetic domains are formed, the reversible motion of domain walls becomes a significant magnetization mechanism, either through a flexural vibration or a wall drift. In view of the characteristic inertia and damping of this movement, wall dynamics is by analogy described by the typical equation for displacement x of driven damped harmonic oscillating systems [12,21]

$$m\frac{d^2x}{dt^2} + \beta\frac{dx}{dt} + ax = 2M_S H e^{j\omega t} \quad (3)$$

where m is the effective wall mass, β the viscous decay or damping coefficient, α the elastic coefficient of the restoring force, H the amplitude of the ac driving magnetic field and ω the driving angular frequency. In order to categorize the response in such systems, the damping ratio $z = \beta/(2\sqrt{m\alpha})$ is used [24].

According to system dynamics, for low damping coefficient, β, so that $z < 1$, the wall motion inertia prevails and the amplitude response exhibits resonance-type frequency dependence in steady-state (underdamped case). Under these conditions, the respective reversible permeability $\mu^*_{dw}(f)$ may be derived from Eq. (3) as

$$\mu^*_{dw}(f) = 1 + \frac{\chi_{0dw}}{1 + jf/f_{dw} - (f/f_R)^2} \quad (4)$$

where $f_{dw} = (2\pi)^{-1}\alpha/\beta$ represents the relaxation frequency and $f_R = (2\pi)^{-1}(\alpha/m)^{1/2}$ the intrinsic vibration frequency or characteristic frequency of the resonance. On the contrary, for large damping coefficient β, so that $z > 1$, the amplitude response of the wall movement shows a relaxation-type steady-state frequency dependence (overdamped or non-oscillatory case).

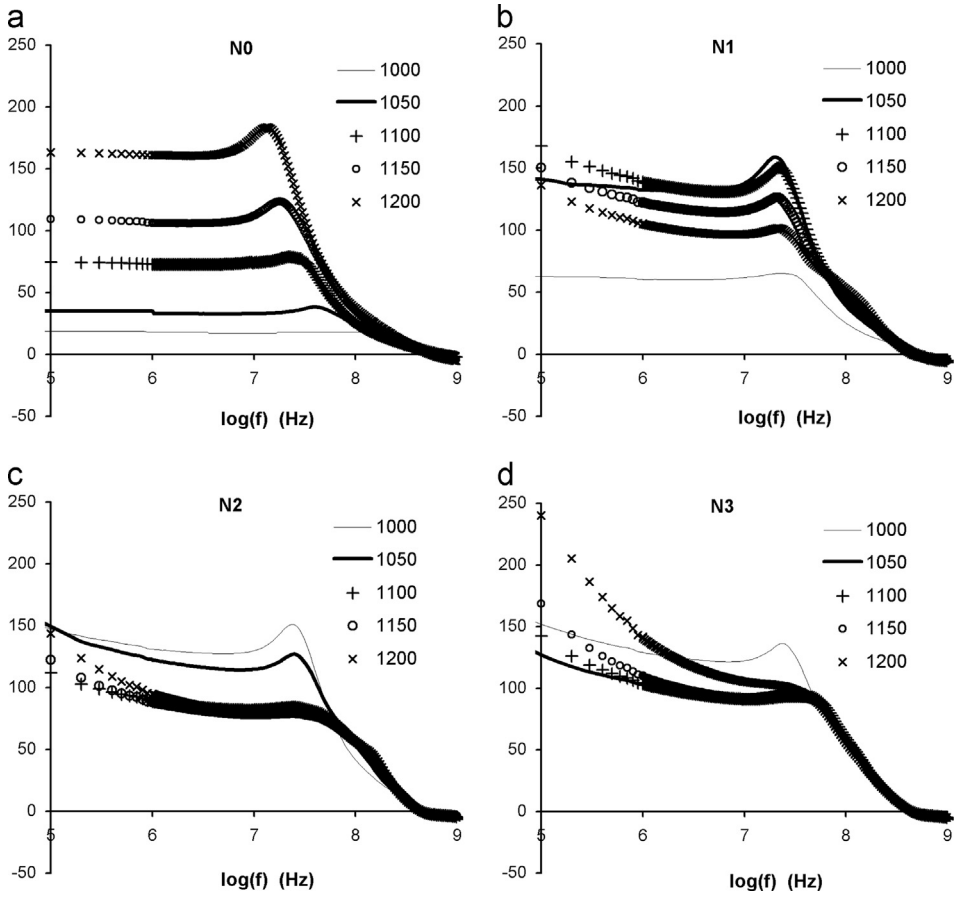

Fig. 8. Frequency dispersion of the real part of magnetic permeability $\mu'(f)$ of samples N0, N1, N2 and N3 sintered at different top temperatures.

3.4. High frequency characterization

As it is important to finally evaluate the high frequency magnetic behavior of the produced NiCuZn ferrites and correlate it with the previously discussed aspects, the real and imaginary parts of complex permeability ($\mu^*(f)=\mu'(f)-j\mu''(f)$) of N0, N1, N2 and N3 were measured in the 100 kHz to 1 GHz range (Figs. 8 and 9).

For the unsubstituted sample N0, both $\mu'(f)$ and $\mu''(f)$ increase substantially and shift to lower frequencies with the increase of T_{SINT}. With regard to the corresponding B–H loops and microstructure images, we assume that N0 sintered at 1000 °C mainly comprises single domain particles in a sparse packing configuration. Consequently, due to the intense demagnetization fields, spin rotation occurs at relatively high frequency (~400 MHz) and this is probably the unique contribution to the magnetization of the sample. Yet, as T_{SINT} is increased, the grains grow further, magnetic domains are formed and some strong resonance-type motion of the domain walls adds up to the permeability spectrum at frequencies just below f_{sp} of spin rotation. While this wall process is significantly enhanced for higher T_{SINT}, the spin rotation is suppressed due to the decrease of the effective anisotropy field.

Concerning the substituted samples N1, N2 and N3, the permeability spectra above 10 MHz are dominated by the overlapping domain wall resonance and spin rotation relaxation curves. Starting from the low-density N1 sample sintered at 1000 °C, permeability is raised for 1050 °C and then is interestingly decreased for higher T_{SINT} values. This progressive decrement is a general remark and becomes more profound for higher Cu content. In fact, the suppression of the wall resonance process takes place simultaneously and in association with the uplift of a relaxation process below 1 MHz. Eventually, the permeability dispersion in the compound N3 sintered at high T_{SINT} mainly consists of two superimposed relaxation mechanisms; the one at low frequencies and magnetization rotation at high frequencies.

In order to comprehend and interpret the variations in the reversible permeability spectrum we employ the notions of elastic domain wall bending and displacement [12,20]. Specifically, although the low-density materials display extended intergranular porosity, they also contain grains developed enough to divide into magnetic domains. Therefore, under the ac excitation field a vibrational motion of the low-energy domain walls is induced, while they remain attached to the grain boundaries (bowing or bulging of domain walls). In Figs. 8 and 9, the contribution of this mechanism is located just below the spin rotation (20–80 MHz). This dynamic behavior is mainly favoured by the microstructure of samples N0 sintered above 1050 °C and N1 sintered up to 1050 °C.

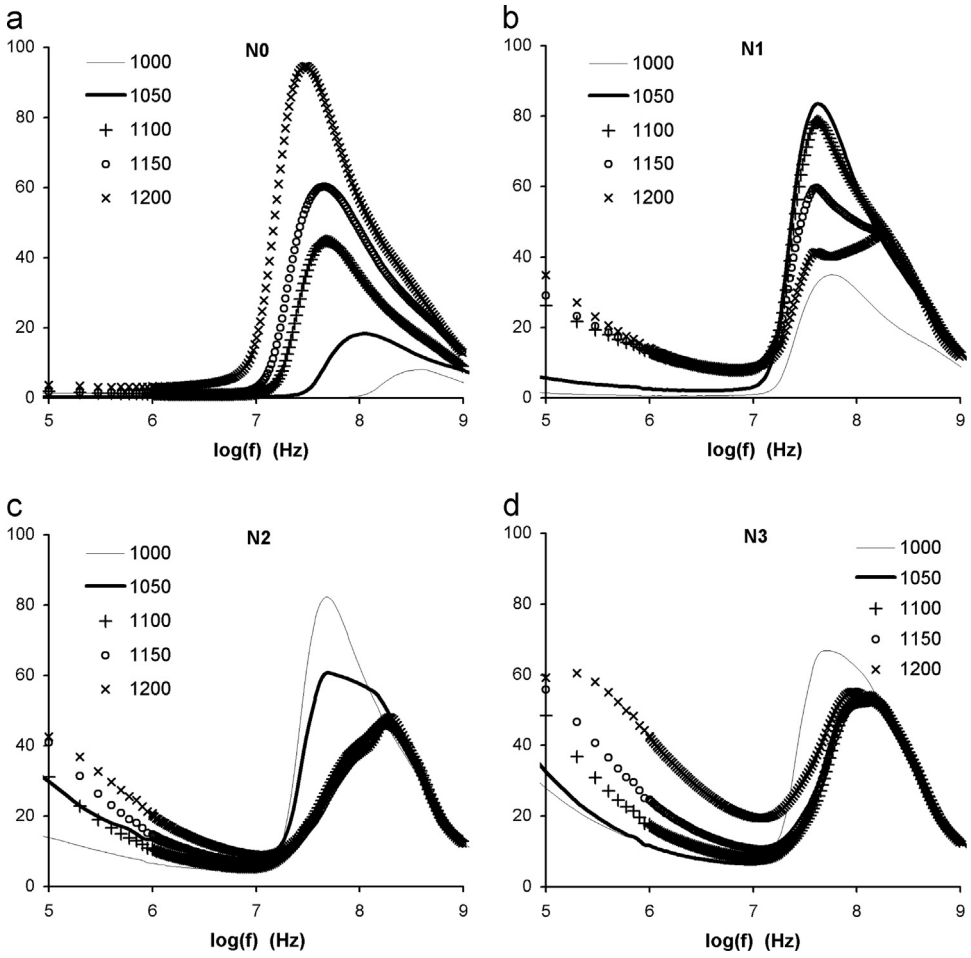

Fig. 9. Frequency dispersion of the imaginary part of magnetic permeability $\mu''(f)$ of samples N0, N1, N2 and N3 sintered at different top temperatures.

As for higher T_{SINT} and Cu substitution the intergranular pores are diminished and grains enlarge, the interfaces between adjacent grains are multiplied, causing the exchange interaction energy and domain wall surface energy to increase. In this microscopic context, the cooperativity between moving walls, introduced by Globus [25], is established and the displacement of rigid higher-energy domain walls is investigated, always in coherence with walls in neighboring grains [12]. Due to the extent of this wall movement, higher decay is expected than the case of wall bowing, giving rise to a relaxation-type permeability dispersion. In Figs. 8 and 9, the low frequency permeability of the substituted samples N1, N2 and N3 arises from the magnetization through domain wall displacement, as it exhibits longer time constant than wall bulging. In order to explore further features of this mechanism, we have drawn the commonly used loss factor $\tan\delta/\mu_i$ of the sample N2 for various T_{SINT} in the range 10 kHz to 1 MHz (Fig. 10). These results reveal that by raising T_{SINT} the magnetic losses are initially increased, followed by a clear drift of the relaxation peak to higher frequency. In fact, as grains grow the domain walls are multiplied and participate in the coherent displacement producing higher μ'_{dw2} and μ''_{dw2}. The subsequent increase in f_{dw2} for 1150 °C and 1200 °C stems by definition from the increase in restoring force α, which shall be attributed to the defects and exerted stresses in larger grains [4,12].

Finally, the contributions of the magnetization processes to the experimental complex permeability spectra were estimated by means of a non-linear least-squares fitting procedure. To this effect, we analyzed the experimental permeability data of samples N0 (Cu: 0) and N3 (Cu: 0.30) sintered at 1100 °C.

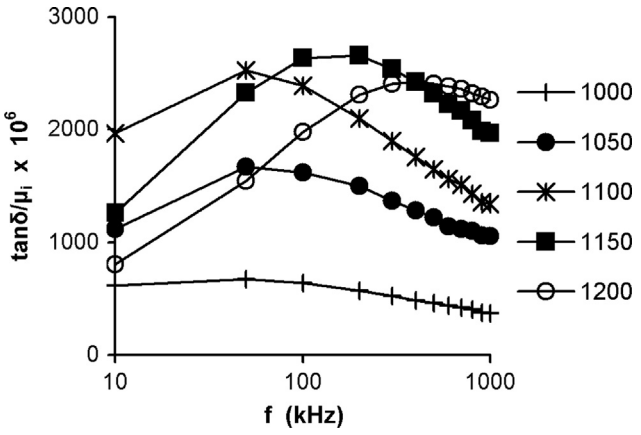

Fig. 10. Frequency variation of loss factor $\tan\delta/\mu_i$ of the sample N2 (Cu: 0.20).

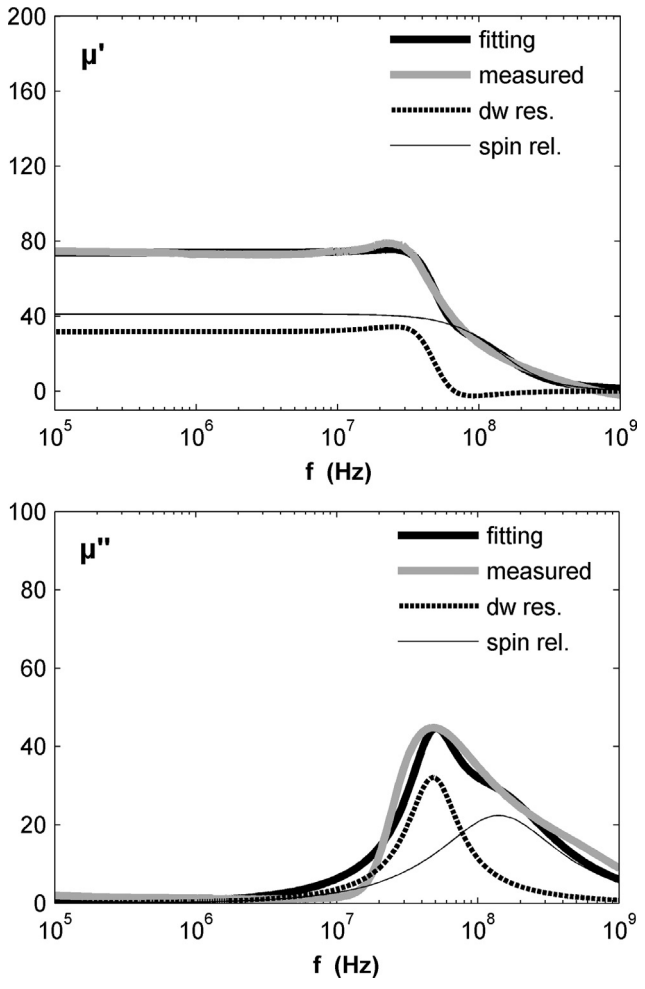

Fig. 11. Fitting of the complex permeability spectrum $\mu^*(f)$ of sample N0 sintered at 1100 °C.

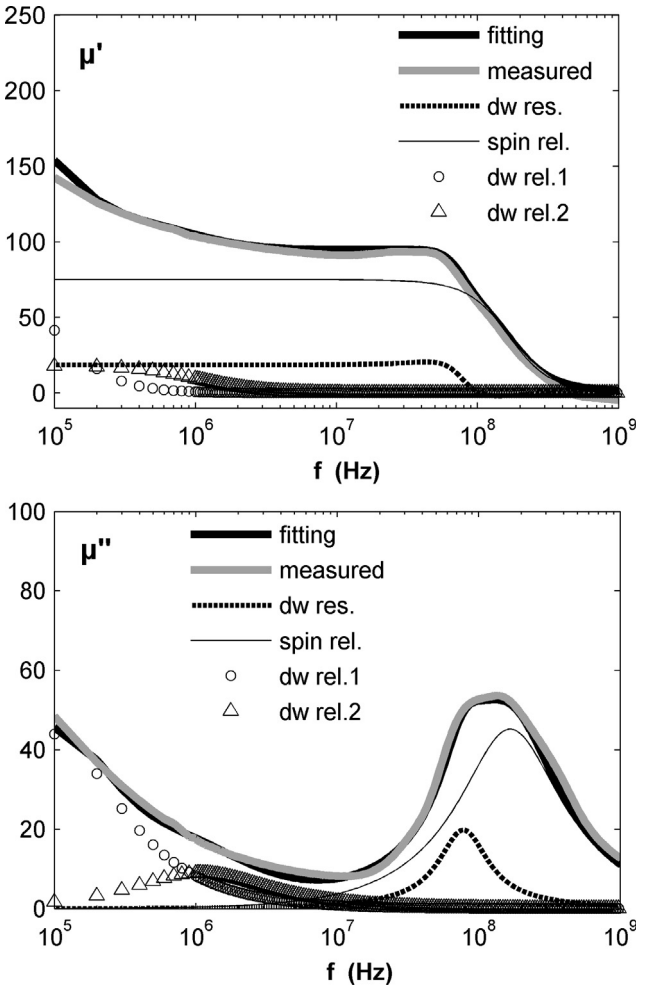

Fig. 12. Fitting of the complex permeability spectrum $\mu^*(f)$ of sample N3 sintered at 1100 °C.

Table 2
The curve-fitting parameters for the permeability spectra of samples N0 and N3. Here, χ_{0sp} and χ_{0dw} are the static susceptibilities, f_{sp} and $f_{dw1,2}$ are the relaxation frequencies (MHz), f_R is the resonance frequency and finally λ and z are the damping parameters of the respective mechanisms.

	Spin rotation				Domain wall bowing			Domain wall displacement				
	χ_{0sp}	f_R	f_{sp}	λ	χ_{0dw}	f_R	z	χ_{0dw}	f_{dw1}	z	χ_{0dw}	f_{dw2}	z
N0	41.1	367.1	76.5	2.4	31.5	64.6	0.54	–			–		
N3	78.0	300.5	100.2	1.5	18.5	99.4	0.49	96.9	0.08	4.8	17.5	1.0	2.5

As this is not a multi-objective algorithm, the curve fitting was performed with reference to the real part of permeability, by using the sum of a proper number of discrete permeability terms calculated by Eqs. (2) and (4). The results of this analysis are demonstrated in Figs. 11 and 12, including the measured and cumulative fitted data along with the proposed constituent curves. In general, the calculated fitting-curves are consistent with the experimental values. Specifically, the permeability spectrum of sample N0 is composed of two curves expressing the spin rotation and domain wall bowing processes. In sample N3, the wall vibration component at ~80 MHz has not completely collapsed, whereas the rise of wall displacement mechanism at frequencies below 10 MHz is effectively described by the superposition of two relaxation processes due to the heterogeneous microstructure. Now, based on the resultant fitting parameters, given in Table 2, the spin rotation susceptibility χ_{sp} is increased in the Cu-substituted sample N3, while the major domain wall contribution shifts from bowing to displacement. These findings are in accordance with the *B–H* measurements and morphological investigation. Moreover, we conclude that the permeability contributions of domain wall bulging and displacement processes are represented by resonance and relaxation-like dispersions, respectively. This accrues from the damping ratio (z) values, whereby we distinguish between the undamped-resonant ($z<1$) and overdamped-relaxing ($z>1$) magnetic response. Concerning the spin component, the optimal overall fitting was attained for $\lambda>1$ implying the damped nature of rotation in both N0 and N3 samples. However as λ is not significantly greater than unity, the loss peak frequency (N0: 140 MHz, N3: 170 MHz) is separated from the respective calculated relaxation frequency f_{sp}. The latter remark basically signifies the necessity for use of the generic Eqs. (2) and (4) in relevant permeability spectrum analysis, instead of simplified relaxation formulas.

4. Conclusions

In the present investigation of the single-phase bulk ferrites $Ni_{0.60-x}Cu_xZn_{0.40}Fe_{1.98}O_4$ with $x=0$, 0.10, 0.20 and 0.30 we have resolved the complex permeability spectra $\mu^*(f)$, in the 100 kHz to 1 GHz frequency range, into three superimposed magnetization components. This analysis indicates the progressively growing contribution of reversible domain wall motion in addition to the initially existent spin rotation process, as the T_{SINT} and the Cu content increase. On that ground, similar variation is displayed by the initial permeability μ_i defined at 10 kHz. Now, particularly with regard to domain wall motion, it is revealed that the substantial magnetizing role of wall bowing, which resonates in the 20–80 MHz area, is taken up by the wall displacement in the below 1 MHz range. This occurs when the sufficiently dense microstructure with large grains enables the formation of cooperative rigid high-energy walls, instead of quasi-isolated pinned low-energy domain walls. Based on the domain wall theory and its system dynamics analog, we distinguish between the low-frequency overdamped relaxation-type wall drift and the higher frequency underdamped resonance-type wall bulging; this distinction along

with the intensity of the three different magnetization processes were verified by least-squares curve fitting of $\mu^*(f)$ for the samples N0 (Cu:0) and N3 (Cu:0.30).

The permeability frequency dispersion is evidently strongly related with the observed sequential transition of microstructure, starting from imperfect low-density and small-grained ferrites until the development of high-density ceramics comprising exaggerated grains with high intragranular porosity. This variation in NiCuZn ferrites is induced by both Cu substitution for Ni and the increase of T_{SINT}. The remarked phenomena allow us to correlate spin rotation with density, whereas the magnetization through domain wall motion is largely affected by both density and grain size distribution. On the basis of the performed *B–H* loop measurements, we notice that raising T_{SINT} prompts the unsubstituted ferrite N0 from single to multiple magnetic domain configurations, while all the substituted ferrites N1, N2 and N3 possess multidomain morphology in the whole T_{SINT} tested range. Thus, in terms of the extracted magnetic properties, the maximum recorded induction B_{MAX} of each sintered sample follows the increasing trend of density, though the coercive field H_C is drastically diminished when domain walls are formed and multiplied.

In conclusion, better insight is offered in the permeability dispersion of spinel ferrites in the high frequency range up to 1 GHz and the capability is provided for manipulation of their magnetic response through compositional and heat treatment control.

References

[1] E. Rezlescu, L. Sachelarie, P.D. Popa, N. Rezlescu, Effect of substitution of divalent ions on the electrical and magnetic properties of Ni–Zn–Me ferrites, IEEE Transactions on Magnetics 36 (2000) 3962–3967.

[2] J. Mürbe, J. Töpfer, Ni–Cu–Zn ferrites for low temperature firing: I. Ferrite composition and its effect on sintering behavior and permeability, Journal of Electroceramics 15 (2005) 215–221.

[3] J.H. Nam, H.H. Jung, J.Y. Shin, J.H. Oh, The effect of Cu substitution on the electrical and magnetic properties of NiZn ferrites, IEEE Transactions on Magnetics 31 (1995) 3985–3987.

[4] D. Sakellari, V. Tsakaloudi, E.K. Polychroniadis, V. Zaspalis, Microstructural phenomena controlling losses in NiCuZn-ferrites as studied by transmission electron microscopy, Journal of the American Ceramic Society 91 (2008) 366–371.

[5] J. Mürbe, J. Töpfer, Low temperature sintering of sub-stoichiometric Ni–Cu–Zn ferrites: shrinkage, microstructure and permittivity, Journal of Magnetism and Magnetic Materials 324 (2012) 578–583.

[6] T. Nakamura, Snoek's limit in high-frequency permeability of polycrystalline Ni–Zn, Mg–Zn, and Ni–Cu–Zn spinel ferrites, Journal of Applied Physics 88 (2000) 348–353.

[7] A. Kriga, D. Allassem, M. Soultan, J.-P. Chatelon, A. Siblini, B. Allard, J.-J. Rousseau, Frequency characterization of thin soft magnetic material layers used in spiral inductors, Journal of Magnetism and Magnetic Materials 324 (2012) 2227–2232.

[8] N.R. Reddy, M.V. Ramana, G. Rajitha, K.V. Sivakumar, V.R.K. Murthy, Stress insensitive NiCuZn ferrite compositions for microinductor applications, Current Applied Physics 9 (2009) 317–323.

[9] T. Kagotani, R. Kobayashi, S. Sugimoto, K. Inomata, K. Okayama, J. Akedo, Magnetic properties and microwave characteristics of Ni–Cu–Zn ferrite film fabricated by aerosol deposition method, Journal of Magnetism and Magnetic Materials 290 (2005) 1442–1445.

[10] R. Dosoudil, M. Ušáková, J. Franek, V. Olah, J. Sláma, E. Ušák, V. Jančárik, Magnetopolymers for EMI suppression in portable and wireless electronics, Journal of Electrical Engineering 57 (2006) 138–141.

[11] J. Smit, H.P.J. Wijn, Ferrites, Philips', Technical Library, Eindhoven, 1959.

[12] D. Jiles, Introduction to Magnetism and Magnetic Materials, second ed., CRC Press LCC, Boca Raton, 1998.

[13] Z.H. Khan, M.M. Rahman, S.S. Sikder, M.A. Hakim, D.K. Saha, Complex permeability of Fe-deficient Ni–Cu–Zn ferrites, Journal of Alloys and Compounds 548 (2013) 208–215.

[14] A.K.M. Akther Hossain, M.L. Rahman, Enhancement of microstructure and initial permeability due to Cu substitution in $Ni_{0.50-x}Cu_xZn_{0.50}Fe_2O_4$ ferrites, Journal of Magnetism and Magnetic Materials 323 (2011) 1954–1962.

[15] T. Tsutaoka, Frequency dispersion of complex permeability in Mn–Zn and Ni–Zn spinel ferrites and their composite materials, Journal of Applied Physics 93 (2003) 2789–2796.

[16] H.-M. Sung, C.-J. Chen, W.-S. Ko, H.-C. Lin, Fine powder ferrite for multilayer chip inductors, IEEE Transactions on Magnetics 30 (1994) 4906–4908.

[17] R.D. Shannon, Revised effective ionic radii and systematic studies of interatomic distances in halides and halcogenides, Acta Crystallographica A32 (1976) 751–767.

[18] A. Goldman, in: Modern Ferrite Technology, Van Nostrand Reinhold, New York, 1990.

[19] B.D. Cullity, C.D. Graham, Introduction to Magnetic Materials, Piscataway, second ed., Wiley-IEEE Press, 2009.

[20] R. Valenzuela, in: Magnetic Ceramics, Cambridge University Press, Cambridge, 1994.

[21] S. Chikazumi, in: Physics of Ferromagnetism, second ed., Oxford University Press, Oxford, 1997.

[22] C. Kittel, Ferromagnetic Resonance, Journal de Physique et Le Radium 132 (1951) 291–302.

[23] A.N. Lagarkov, K.N. Rozanov, N.A. Simonov, S.N. Starostenko, Microwave Permeability of Magnetic Films, Springer, New York, 2006.

[24] K. Ogata, System Dynamics, fourth ed., Pearson Prentice Hall, Upper Saddle River, 2004.

[25] A. Globus, Some physical considerations about the domain wall size theory of magnetization mechanisms, Journal de Physique Colloques 38 (1977) C1-1–C1-15.